

## SPECTRA OF HIGH-REDSHIFT TYPE Ia SUPERNOVAE AND A COMPARISON WITH THEIR LOW-REDSHIFT COUNTERPARTS<sup>1</sup>

I. M. HOOK,<sup>2</sup> D. A. HOWELL,<sup>3</sup> G. ALDERING,<sup>4</sup> R. AMANULLAH,<sup>5</sup> M. S. BURNS,<sup>6</sup> A. CONLEY,<sup>4,7</sup> S. E. DEUSTUA,<sup>8</sup>  
R. ELLIS,<sup>9</sup> S. FABBRO,<sup>10</sup> V. FADEYEV,<sup>4</sup> G. FOLATELLI,<sup>5</sup> G. GARAVINI,<sup>5,11</sup> R. GIBBONS,<sup>12</sup> G. GOLDBABER,<sup>4,7</sup>  
A. GOOBAR,<sup>5</sup> D. E. GROOM,<sup>4</sup> A. G. KIM,<sup>4</sup> R. A. KNOP,<sup>12</sup> M. KOWALSKI,<sup>4</sup> C. LIDMAN,<sup>13</sup> S. NOBILI,<sup>5,11</sup>  
P. E. NUGENT,<sup>4</sup> R. PAIN,<sup>11</sup> C. R. PENNYPACKER,<sup>4</sup> S. PERLMUTTER,<sup>4,7</sup> P. RUIZ-LAPUENTE,<sup>14</sup>  
G. SAINTON,<sup>11</sup> B. E. SCHAEFER,<sup>15</sup> E. SMITH,<sup>12</sup> A. L. SPADAFORA,<sup>4</sup> V. STANISHEV,<sup>5</sup>  
R. C. THOMAS,<sup>4</sup> N. A. WALTON,<sup>16</sup> L. WANG,<sup>4</sup> AND W. M. WOOD-VASEY<sup>4,7</sup>

(THE SUPERNOVA COSMOLOGY PROJECT)

Received 2005 February 9; accepted 2005 August 3

### ABSTRACT

We present spectra for 14 high-redshift ( $0.17 < z < 0.83$ ) supernovae, which were discovered by the Supernova Cosmology Project as part of a campaign to measure cosmological parameters. The spectra are used to determine the redshift and classify the supernova type, essential information if the supernovae are to be used for cosmological studies. Redshifts were derived either from the spectrum of the host galaxy or from the spectrum of the supernova itself. We present evidence that these supernovae are of Type Ia (SNe Ia) by matching to spectra of nearby supernovae. We find that the dates of the spectra relative to maximum light determined from this fitting process are consistent with the dates determined from the photometric light curves, and, moreover, the spectral time sequences for SNe Ia at low and high redshift are indistinguishable. We also show that the expansion velocities measured from blueshifted Ca H and K are consistent with those measured for low-redshift SNe Ia. From these first-level quantitative comparisons we find no evidence for evolution in SN Ia properties between these low- and high-redshift samples. Thus, even though our samples may not be complete, we conclude that there is a population of SNe Ia at high redshift whose spectral properties match those at low redshift.

*Key words:* distance scale — stars: distances — supernovae: general

*Online material:* color figures

### 1. INTRODUCTION

The peak magnitudes of Type Ia supernovae (SNe Ia) are one of the best distance indicators at high redshifts, where few reliable distance indicators are available to study the cosmological parameters. Beginning with the discovery of SN 1992bi (Perlmutter et al. 1995), the Supernova Cosmology Project (SCP) has developed search techniques and rapid analysis methods that allow systematic discovery and follow up of “batches” of high-redshift SNe. These searches and those of the High- $z$  SN Team have resulted in  $\sim 100$  published SNe ( $0.15 < z < 1.2$ ), which have been used for measurements of the cosmological parameters  $\Omega_M$  and  $\Omega_\Lambda$  and to provide initial constraints on the equation of state of the universe,  $w$  (Perlmutter et al. 1998, 1999; Schmidt et al.

1998; Garnavich et al. 1998; Riess et al. 1998, 2004; Knop et al. 2003; Barris et al. 2004; Tonry et al. 2003).

Spectra have been obtained for as many of the SCP SNe as possible and as close as possible to maximum light. The spectra are used to determine the redshift of the event and to confirm its spectral subtype, both crucial if the SN is to be used in a determination of cosmological parameters. In addition, the spectra provide a check that SNe Ia at high redshift are similar to those at low redshift, an assumption central to the use of SNe Ia as “standard candles.” This paper represents a significant contribution to the amount of published high-redshift SN Ia spectroscopy (Lidman et al. 2005; Barris et al. 2004; Tonry et al. 2003; Coil et al. 2000; Matheson et al. 2005).

In this paper we present spectra for a subset of our distant SNe, discovered during search campaigns in 1997 January and

<sup>1</sup> Much of the data presented herein were obtained at the W. M. Keck Observatory, which is operated as a scientific partnership among the California Institute of Technology, the University of California, and the National Aeronautics and Space Administration. The Observatory was made possible by the generous financial support of the W. M. Keck Foundation. Also based in part on observations made with the European Southern Observatory telescopes (ESO programs 58.A-0745 and 59.A-0745).

<sup>2</sup> Department of Physics, University of Oxford, Nuclear and Astrophysics Laboratory, Keble Road, Oxford OX1 3RH, UK.

<sup>3</sup> Department of Astronomy and Astrophysics, University of Toronto, 60 St. George Street, Toronto, ON M5S 3H8, Canada.

<sup>4</sup> E. O. Lawrence Berkeley National Laboratory, 1 Cyclotron Road, Berkeley, CA 94720.

<sup>5</sup> Department of Physics, Stockholm University, AlbaNova University Center, SE-106 91 Stockholm, Sweden.

<sup>6</sup> Colorado College, 14 East Cache La Poudre Street, Colorado Springs, CO 80903.

<sup>7</sup> Department of Physics, University of California, Berkeley, CA 94720-7300.

<sup>8</sup> American Astronomical Society, 2000 Florida Avenue NW, Suite 400, Washington, DC 20009.

<sup>9</sup> California Institute of Technology, 1200 East California Boulevard, Pasadena, CA 91125.

<sup>10</sup> Centro Multidisciplinar de Astrofísica (CENTRA), and Departamento de Física, IST, Lisbon, Portugal.

<sup>11</sup> Laboratoire de Physique Nucléaire et de Hautes Energies, CNRS-IN2P3, University of Paris VI and VII, Paris, France.

<sup>12</sup> Department of Physics and Astronomy, Vanderbilt University, Nashville, TN 37240.

<sup>13</sup> European Southern Observatory, Alonso de Cordova 3107, Vitacura, Casilla 19001, Santiago 19, Chile.

<sup>14</sup> Department of Astronomy, University of Barcelona, Barcelona, Spain.

<sup>15</sup> Department of Physics and Astronomy, Louisiana State University, Baton Rouge, LA 70803.

<sup>16</sup> Institute of Astronomy, Madingley Road, Cambridge CB3 0HA, UK.

March. Since the goal of this paper is a first quantitative comparison of high- and low-redshift SN spectra, spectra were chosen where the SN features were relatively clear. Spectra of 33 objects were taken during the two campaigns, of which four were found to be clear, broad-lined QSOs and two were “featureless” blue objects (possibly BL Lac objects) for which a redshift could not be measured. The other objects all have measured redshifts, and of these about half (13) were rejected for the purposes of this paper based on one or both of the following criteria: low signal-to-noise ratio (S/N) (i.e., less than about 10 per 20 Å bin over the observed wavelength range 6000–8000 Å) or large contamination by the host galaxy, roughly corresponding to a percentage increase of less than 50% in  $R$ -band photometry between reference and “new” images (although the latter is only a rough guide, since the phase of the SN, its location relative to the core of the galaxy, and the seeing all strongly affect how clearly the SN appears in the spectrum).

The spectra presented here provide the basis for the identification of these objects as Type Ia, as quoted in Perlmutter et al. (1999) and Knop et al. (2003). Future papers by Garavini et al. (2005) and E. Smith et al. (2006, in preparation) will present spectroscopic results and analysis of other SCP data sets.

For each object in our sample we give the redshift and present the results of matching the spectrum to various SN templates (including SNe of types other than Ia) and hence give spectroscopic evidence that these distant SNe are of Type Ia. The spectral dates derived from this matching process are compared with the dates derived from the light curves. Finally, we present the set of high-redshift SN spectra as a time sequence showing that the spectrum changes with light-curve phase in a similar way at low and high redshift.

## 2. DISCOVERY OF THE SUPERNOVAE

The observing strategy developed for these high-redshift SN search runs involved comparison of large numbers of galaxies in each of  $\sim 50$   $14'.7 \times 14'.7$  fields observed twice with a separation of 3–4 weeks (Perlmutter et al. 1997). This strategy ensures that almost all the SNe are discovered before maximum light, and, since it could be guaranteed that at least a dozen SNe would be found on a given search run, the follow-up observing time could be scheduled in advance. This strategy made it possible to schedule spectroscopy time on large telescopes while the SNe were still close to maximum light; thus, the SN features can be observed even at redshifts  $>1$ . Follow-up photometric measurements were also made of the SN light curves, from which the maximum brightness and date of maximum are derived.

The SNe described in this paper were identified on  $R$ -band images taken in two searches on the Cerro Tololo Inter-American Observatory (CTIO) 4 m Blanco telescope in 1997 January and March. Candidate SNe were identified on the difference images (see Perlmutter et al. [1997] for details on the identification of candidates). Those SNe identified as Type Ia were followed up photometrically in the  $R$  and  $I$  bands at the WIYN telescope at Kitt Peak National Observatory and the ESO 3.6 m telescope, and one (SN 1997ap) was followed up with the *Hubble Space Telescope* (Perlmutter et al. 1998).

Parameterized light-curve fits for all but one of the objects presented in this paper (SN 1997ag, which does not have sufficient photometric light-curve measurements for cosmological use) are published in Perlmutter et al. (1999). These SNe form part of the set that provided the first evidence for the accelerating expansion of the universe and the presence of some form of dark energy driving this expansion. Many of these objects (but excluding SN 1997ag, SN 1997G, SN 1997J, and SN 1997S be-

TABLE 1  
SUMMARY OF SPECTRAL OBSERVATIONS

IAU Name	$R^a$ (mag)	Telescope	Exposure (hr)	Date (UT)
1997F.....	23.9	Keck II	1.0	1997 Jan 12
1997G.....	23.7	Keck II	1.3	1997 Jan 13
1997I.....	20.9	ESO 3.6 m	1.0	1997 Jan 13
1997J.....	23.4	Keck II	1.3	1997 Jan 13
1997N.....	21.0	ESO 3.6 m	0.5	1997 Jan 13
1997R.....	24.4	Keck II	1.4	1997 Jan 13
1997S.....	23.6	Keck II	1.8	1997 Jan 13
1997ac.....	23.1	Keck II	0.17	1997 Mar 14
1997af.....	23.8	Keck II	0.58	1997 Mar 14
1997ag.....	23.2	Keck II	0.25	1997 Mar 14
1997ai.....	22.3	Keck II	0.35	1997 Mar 13
1997aj.....	22.3	Keck II	0.67	1997 Mar 13
1997am.....	22.9	Keck II	0.31	1997 Mar 13
1997ap.....	24.2	Keck II	1.5	1997 Mar 14

<sup>a</sup> The magnitudes given are for the SNe at the time of the spectroscopic observations and were estimated from nearby light-curve photometry points. These are accurate to about 0.2 mag.

cause of poor color measurements,  $\sigma_{R-I} > 0.25$ ) were also used in the more recent measurements of cosmological parameters by Knop et al. (2003).

## 3. SPECTROSCOPIC OBSERVATIONS

The spectra were obtained during two observing runs at the Keck II 10 m telescope (two nights in 1997 January and three in 1997 March) and one run at the ESO 3.6 m (one night in 1997 January). The spectroscopic runs were scheduled to occur within 1 week of the corresponding search run at CTIO. At the time of the observations, close to maximum light, the typical magnitudes of the SN candidates were 22–24 mag in the  $R$  band, and, in many cases, their host galaxies had similar apparent magnitudes. In all cases in which the galaxy was bright enough, the slit was aligned at a position angle on the sky such that the SN and the center of the host galaxy were both in the slit. This was done to allow redshift determination from features in the host galaxy spectrum. Table 1 gives the dates and exposure times for the observations of the various SN candidates.

Observations of the spectrophotometric standards HD 84937, HD 19445, and BD 262606 (Oke & Gunn 1983) were taken at Keck II, and LTT 1788 (Stone & Baldwin 1983; Baldwin & Stone 1984; Hamuy 1994) was observed at ESO, in order to obtain approximate relative flux calibration of the spectra. The standards were observed at the parallactic angle, but note that the SN spectra were not necessarily taken at the parallactic angle as described above. Although the effects of atmospheric dispersion are small when observing in the red (as is the case for these spectra), some small wavelength-dependent slit losses may occur. Therefore, the overall slope of the spectra is not considered to be reliable, and the slope is left as a free parameter in the analysis that follows.

*Keck data.*—The Low Resolution Imaging Spectrometer spectrograph (Oke et al. 1995) with the 300 lines  $\text{mm}^{-1}$  grating was used at the Cassegrain focus of the Keck II 10 m telescope. The spectra cover the wavelength range 5000–10000 Å with dispersion of  $\sim 2.5$  Å  $\text{pixel}^{-1}$ . Typical exposure times were 0.5–1.5 hr.

During the January run, dome flats were taken at the position of targets when possible. This was necessary because flexure causes the fringe pattern to shift depending on the zenith distance and rotator angle. Previous tests showed that dome flats gave marginally

better results compared to internal flats when trying to subtract sky lines at the red end of the spectrum. During the March run, bad weather and technical problems severely limited the amount of usable time. Therefore, to allow us to observe all the candidates, the exposure times for each object were reduced, and only internal flats were taken. HgNeAr arc spectra for wavelength calibration were obtained at the same position as the flats.

*ESO 3.6 m data.*—The ESO Faint Object Camera and Spectrograph 1 (Buzzoni et al. 1984) was used at the Cassegrain focus of the ESO 3.6 m. The R300 grism was used, giving a dispersion of  $3.5 \text{ \AA pixel}^{-1}$  over the range 5900–10000 Å. Dome flats were used to flat-field the data, and wavelength calibration was carried out using observations of HeAr (ESO) arc lamps.

#### 4. DATA REDUCTION

The spectra were reduced using the IRAF<sup>17</sup> spectral reduction package. The data were first overscan-subtracted, bias-corrected, and flat-fielded using the flats described above. The spectra were then extracted to provide one-dimensional spectra of the targets. In some cases the SN was sufficiently offset from the core of its host galaxy that it was possible to extract the SN spectrum and that of the host galaxy separately. In other cases it was only possible to extract a single spectrum containing a mix of SN and host galaxy light. These spectra were then wavelength- and flux-calibrated. Except where otherwise stated explicitly, a correction for atmospheric absorption features was made.

#### 5. IDENTIFICATION

SNe Ia are classified spectroscopically by a lack of hydrogen and the presence of a strong Si II feature at  $\sim 6150 \text{ \AA}$  in the rest frame (see Filippenko [1997] for a review). However, at redshifts above 0.5, this line moves into the infrared and can no longer be seen with typical CCDs. Therefore, we use the following criteria to classify a spectrum as a SN Ia when this line is not seen:

1. Presence of the S II “W” feature at  $\sim 5500 \text{ \AA}$ . This is only seen in SNe Ia (see Fig. 1).
2. Presence of the Si II feature at  $\sim 4000 \text{ \AA}$ . If seen, this feature indicates that the SN is definitely of Type Ia, although for spectra prior to maximum light or for SN 1991T-like SNe Ia, this feature can be weak. Note that it is easy to mistake Ca H and K from the host galaxy for this feature.
3. The combination of the light-curve age with the temporal evolution of the Fe II features at  $\sim 4500$  and  $5100 \text{ \AA}$ . In a SN Ib/c at maximum light, these Fe II features resemble those in a SN Ia about 2 weeks after maximum light (Fig. 1), but the appearance of a Type Ia spectrum at maximum light is unique.

##### 5.1. Matching Technique

The spectra in this paper were matched against template SN spectra using a spectrum matching code developed by Howell & Wang (2002). All fits were performed after rebinning the data to  $20 \text{ \AA}$  to allow more rapid runs of the fitting program. At a given redshift, the code computes

$$\chi^2 = \frac{w(\lambda)[O(\lambda) - aT(\lambda)10^{cA_\lambda} - bG(\lambda)]^2}{\sigma(\lambda)^2},$$

<sup>17</sup> IRAF is distributed by the National Optical Astronomy Observatory, which is operated by the Association of Universities for Research in Astronomy (AURA), Inc., under cooperative agreement with the National Science Foundation.

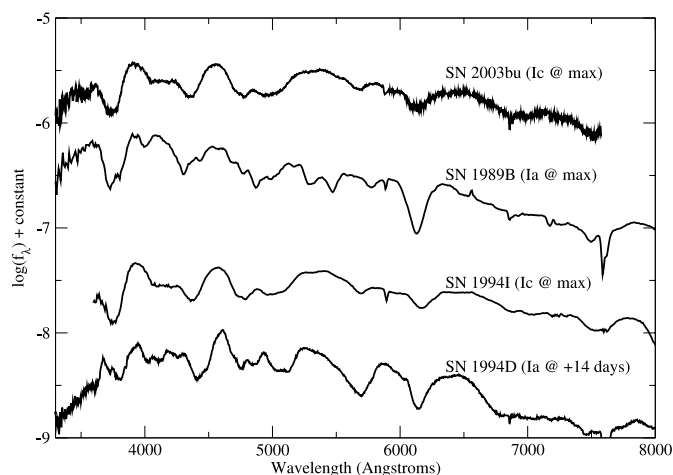


FIG. 1.—Comparison of nearby SNe Ia and Ic at maximum light. SNe Ic can closely resemble SNe Ia blueward of  $4500 \text{ \AA}$ , with the exception of the  $4000 \text{ \AA}$  Si II feature. Also, SNe Ic have a group of Fe features spanning  $4500\text{--}5200 \text{ \AA}$  that resemble the same features in a Type Ia spectrum  $\sim 2$  weeks after maximum light. The data shown are SN 1989B (Wells et al. 1994), SN 2003bu (P. Nugent 2005, private communication), SN 1994I (Clocchiatti et al. 1996), and SN 1994D (Meikle et al. 1996).

where  $w(\lambda)$  is a weighting function,  $O$  is the observed spectrum,  $T$  is the SN template spectrum,  $G$  is the host galaxy template spectrum,  $A_\lambda$  is the reddening law,  $\sigma$  is the error on the spectrum, and  $a$ ,  $b$ , and  $c$  are constants that are varied to find the best fit. The weighting function was set to be unity across the spectrum except at the telluric features, which were given zero weight. This equation is iterated over a range of redshifts to find the minimum  $\chi^2$  in redshift, host galaxy, template SN, and reddening space. In this analysis, the reddening law (Cardelli et al. 1989; O’Donnell 1994) was fixed at  $R_V = 3.1$ , although the spectrum matching code can handle other values of  $R_V$ .

When the redshift was well determined from narrow galaxy lines, it was constrained in the fits. Likewise, when the host galaxy type was known from Sullivan et al. (2003), it was fixed in the following manner. For Sullivan type 0, E and S0 galaxies were tested. For type 1, Sa and Sb galaxies were allowed, and for type 2, Sb, Sc, and starburst galaxy types were used. The galaxy templates subtracted here were those of Kinney et al. (1993), which have been smoothed and had their narrow lines removed.

In three cases, SN 1997ac, SN 1997ai, and SN 1997ap, it was not possible to obtain a host galaxy redshift. In these cases the redshift was determined from fits to SN templates. For each template, the best-fit redshift was determined by stepping through redshift space in 0.001 increments. In § 5.3 we describe the estimation of redshift uncertainties for these cases.

The fitting program is intended to aid human classifiers of SN spectra—it is not a replacement for them. The program returns a list of fits in decreasing order of goodness of fit. The output is inspected, and a “best fit” is chosen. A good indication of the level of certainty of a match is the amount of agreement between the best fits. For data with good S/N and little host contamination, there is almost always excellent agreement between the top five fits.

The program is also limited by the available template data. For example, less than a dozen SNe have UV spectroscopy near or before maximum light (Cappellaro et al. 1995), and core-collapse SNe are particularly underrepresented in terms of UV observations. Thus, at high redshift, where the observed optical band corresponds to rest-frame UV, it can be hard to obtain

TABLE 2  
LIST OF THE NEARBY SUPERNOVAE USED AS TEMPLATES  
IN THE FITTING PROCEDURE

SN Type	SN Name
Ia .....	1981B, 1986G, 1989B, 1990N, 1991T, 1991bg, 1992A, 1994D, 1996X, 1998bu, 1999aa, 1999ac, 1999ao, 1999av, 1999aw, 1999be, 1999bk, 1999bm, 1999bn, 1999bp, 1999ec
II.....	1979C, 1980K, 1984E, 1986I, 1987A, 1987B, 1987K, 1988A, 1988Z, 1993J, 1993W, 1997cy, 1999em, 1999em <sup>a</sup>
Ibc .....	1983N, 1983V, 1984L, 1987M, 1988L, 1990B, 1990U, 1990aa, 1991A, 1991K, 1991L, 1991N, 1991ar, 1994I, 1995F, 1995bb, 1996cb, 1997C, 1997dd, 1997dq, 1997ei, 1997ef, 1998bw, 1998dt, 1999P, 1999bv, 1999di, 1999dn, 1999ex, 2000H

NOTES.—Details of the dates of these spectra and their references will be presented by D. A. Howell (2006, in preparation). The SUSPECT SN archive (Richardson et al. 2002) was used in the creation of this library.

<sup>a</sup> Theoretical SN 1999em spectra provided by P. Nugent.

conclusive results. One other problem area is at very early times. From day  $-18$  to  $-8$  there are few spectra of SNe Ia, and these are the epochs in which SNe Ia show the greatest diversity. Furthermore, Si II  $\lambda 4000$  can be weak or absent at very early times, making a secure classification difficult. Finally, after a week past maximum light, SNe Ib/c and SNe Ia show the greatest similarity in their spectra (see Fig. 1). We note that more UV spectra of SNe Ib/c would be beneficial to the classification process. With such spectra it would be possible to confirm some cases that are probable Type Ia but for which Type Ib/c cannot be eliminated. If Si II  $\lambda 6150$  is not in the observed spectral range, or there is host contamination, classification at this phase can be harder than at other phases. The list of nearby SNe used in the fitting process is given in Table 2. A full list of the dates of

these spectra and their references will be presented by D. A. Howell (2006, in preparation).

Near maximum light, normal SNe Ia show a characteristic pattern of absorption features at rest frame 3800 Å (Ca II), 4000 Å (Si II), 4300 Å (Mg II and iron peak lines), 4900 Å (various iron peak lines), 5400 Å (S II “W”), 5800 Å (Si II and Ti II), and 6150 Å (Si II). If the S/N of the spectrum is low, typical Type Ia indicator lines such as Si II and S II may be hard to identify definitively. However, the overall pattern of features in a SN Ia at a given epoch is unique, so fits to the overall spectrum (with sufficient S/N) can allow a secure classification of the SN type, especially when there is an independent confirmation of the SN epoch from the light curve.

In summary, this procedure provides a more robust measurement of the SN type than unaided human typing by eye. Furthermore, it uses the shape of the entire spectrum to classify SNe, not just one or two key features. The technique also provides a spectroscopic determination of the rest-frame date the spectrum was taken (relative to maximum light), which can be checked against the light curve, yielding an independent consistency check, as shown in § 5.2.

### 5.2. Matching Results

The results of the fitting procedure are given in Table 3. We show the best-fit SN template, the type of host galaxy that was subtracted (if any), the redshift, and the epoch of the template spectrum. In addition, we give a “spectroscopic epoch,” which is the weighted average of the epochs from the five best-fit spectra. This spectroscopic determination of the epoch of the SN can be compared with the epoch determined from the light curve, also presented in Table 3. Figure 2 shows that the two numbers are in good agreement, with an rms difference of 3.3 days.

The program also formally returns an estimate of the amount of reddening (or dereddening) required to match the observed

TABLE 3  
SUMMARY OF FITTING RESULTS

IAU Name	$z$	$\tau_{lc}^a$	$\tau_s^b$	$\tau_t^c$	Match	G <sup>d</sup>	G <sup>e</sup>
1997F .....	0.580 ± 0.001	-7.5 ± 0.4	-6.5 ± 4.1	-8	1999ec	1	Sa
1997G.....	0.763 ± 0.001	+5.4 ± 1.0	+0.7 ± 5.1	+4	1999bk	2	...
1997I.....	0.172 ± 0.001	-3.3 ± 0.1	+1.2 ± 1.5	+1	1999bp	1	Sb
1997J.....	0.619 ± 0.001	+3.6 ± 1.1	+0.7 ± 4.0	+2	1999bn	0	S0
1997N.....	0.180 ± 0.001	+15.0 ± 0.1	+16.7 ± 2.3	+15	1991T	2	Sb2
1997R.....	0.657 ± 0.001	-5.6 ± 0.4	+0.0 ± 3.1	-5	1989B	1	Sa
1997S.....	0.612 ± 0.001	+2.1 ± 0.7	+3.3 ± 2.1	+5	1992A	...	Sb1
1997ac.....	0.323 ± 0.005 <sup>f</sup>	+9.4 ± 0.1	+11.9 ± 3.4	+11	1998bu	...	...
1997af.....	0.579 ± 0.001	-5.3 ± 0.3	+1.3 ± 6.2	-2	1999bp	2	Sb6
1997ag.....	0.592 ± 0.001	-1.7 ± 2.0 <sup>g</sup>	+1.9 ± 6.0	-7	1990N	...	Sa
1997ai.....	0.454 ± 0.006 <sup>f</sup>	+5.2 ± 0.7	+4.8 ± 1.8	+5	1992A	...	...
1997aj.....	0.581 ± 0.001	-4.4 ± 0.3	-0.7 ± 7.5	-3	1999aa	2	Sb
1997am.....	0.416 ± 0.001	+10.0 ± 0.5	+7.4 ± 2.9	+9	1992A	2	Sb1
1997ap.....	0.831 ± 0.007 <sup>f</sup>	-2.3 ± 0.5	+0.3 ± 3.6	-5	1989B	2	...

<sup>a</sup> Spectral epoch relative to  $B$  light-curve maximum (in the rest frame) as determined from light-curve fitting (Knop et al. 2003).

<sup>b</sup> Spectral epoch from weighted average of five best-fit spectra. The uncertainty quoted is the weighted standard deviation of the epochs of the five best SN Ia fits.

<sup>c</sup> Spectral epoch of best matching comparison template spectrum.

<sup>d</sup> Host galaxy type from Sullivan et al. (2003): 0, E-S0; 1, Sa-Sb; and 2, Sc and later.

<sup>e</sup> Template host galaxy spectrum subtracted from the data for the fits.

<sup>f</sup> Redshift determined from the SN alone. These values are derived based on the matching procedure described in § 5.1 and supersede those in Perlmutter et al. (1999) and Knop et al. (2003). The uncertainties in these redshifts were estimated as described in § 5.3.

<sup>g</sup> This SN has a poorly constrained light curve, because only a small number of photometric measurements were made. In order to estimate the time of maximum, it was necessary to constrain the stretch parameter to  $s = 1$  when fitting the light curve.

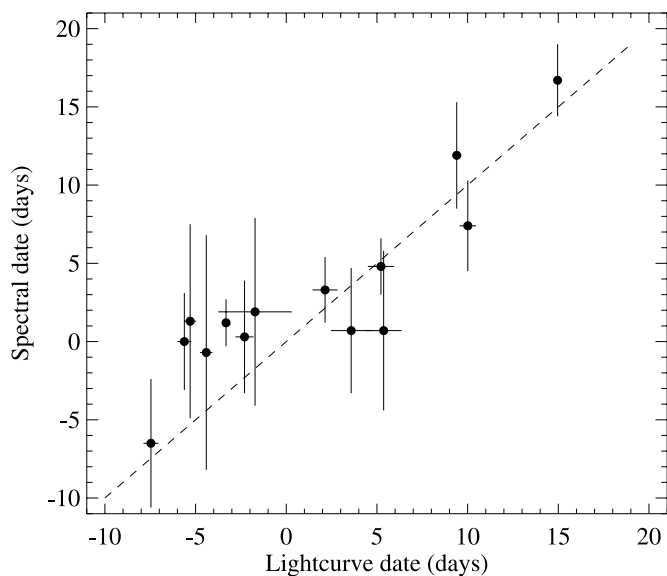


FIG. 2.—Comparison of the epoch of the spectrum as determined from the light curve ( $\tau_{lc}$ ) with that determined from the weighted average of the five best template fits to the spectrum ( $\tau_s$ ). In both cases the epochs are expressed as rest-frame days relative to maximum light. The dashed line shows the locus  $\tau_{lc} = \tau_s$ .

spectrum, but this number may not reflect the actual reddening toward the SN. This parameter accounts for all differences in color between the observation and the template, so differential slit losses due to observations not taken at the parallactic angle, wavelength-dependent seeing, errors in flux calibration, and uncorrected reddening in the templates all make an accurate determination of the reddening to the SN from this spectroscopy alone unfeasible.

### 5.3. Measurement of Redshifts

In most cases the slit angle for the spectroscopic observations was chosen so that light from both the SN and the host galaxy (when visible on the CTIO images) fell down the slit. Since features in the galaxy spectra are typically much narrower than those in the SN spectra, it is often possible to obtain a redshift from the galaxy features, even in cases in which the SN and host galaxy light are blended. Table 3 summarizes the measured redshifts.

In the cases in which galaxy features were visible, the centroids of the lines were measured and the redshift calculated by taking the mean of the redshifts derived from the individual lines. The uncertainty in the mean redshift  $z$  is estimated as  $\pm 0.001$ .

In the cases in which there were no identifiable host galaxy features to determine the redshift (SN 1997ac, SN 1997ai, and SN 1997ap), the redshift was determined from fits to SN templates as described in § 5.1. In order to estimate the uncertainty in these redshifts, we used the other 11 cases, whose redshifts were known from the host galaxies, as follows. Each high-redshift spectrum was cross-correlated with the corresponding best-fit template (using the IRAF cross-correlation routine *fxcor*), allowing redshift to vary. In this sample of 11 cases, we found a mean redshift difference between SN and host redshift of  $-0.0012$  and an rms difference of  $0.005$ . Thus, there does not appear to be any significant systematic redshift error, and the uncertainty in redshift is about  $0.005$ . This test measures the uncertainty in redshift determination when the “correct” template is used. For cases in which the redshift is not known from

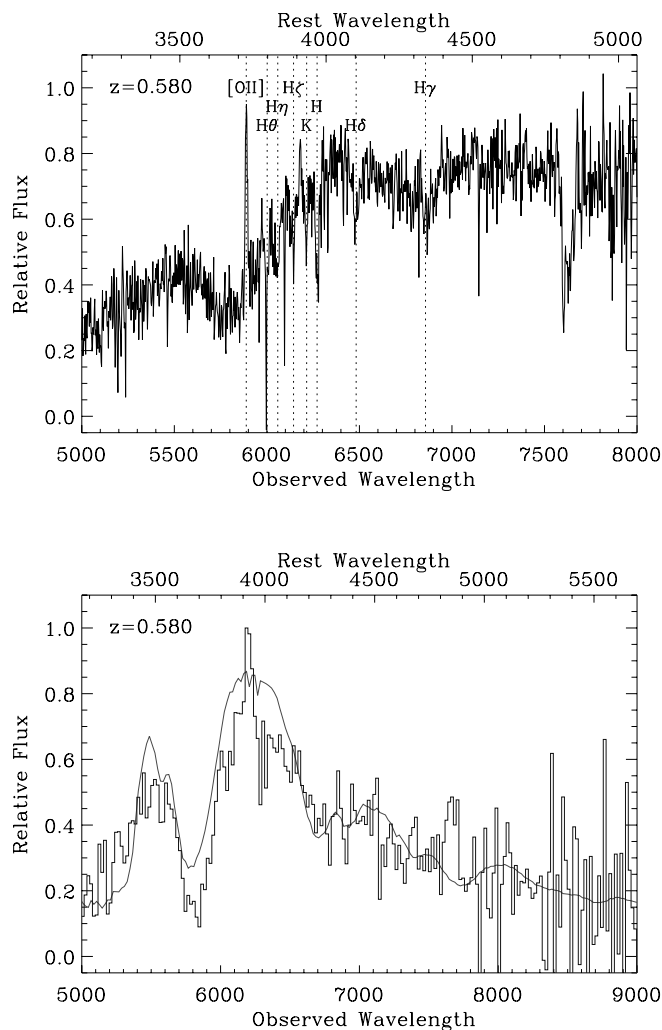


FIG. 3.—*Top*: Unsmoothed spectrum of SN 1997F showing narrow features used to determine the redshift (note that atmospheric absorption has not been corrected in this spectrum). *Bottom*: Rebinned spectrum of SN 1997F (histogram) after interpolating over narrow galaxy lines and the sky absorption feature at  $7600 \text{ \AA}$  and subtracting a template Sa galaxy, compared with SN 1999ee at  $-8$  days (solid curve). [See the electronic edition of the Journal for a color version of the bottom panel.]

the host galaxy, there is an additional uncertainty from the diversity of velocities seen in nearby template spectra. To estimate the size of this effect we took the standard deviation of the velocity of the Si II  $\lambda 6150$  feature for the SNe Ia presented in Benetti et al. (2005). Our calculated value of  $1300 \text{ km s}^{-1}$  corresponds to a redshift uncertainty of  $0.004$ . Combining these two effects in quadrature gives an estimated uncertainty in redshift of about  $0.006$  on average. However, we also note that the uncertainties should increase with redshift (and, indeed, this general trend is seen in our sample of 11 objects), because the lines become broader, the S/N becomes poorer, and the spectrum corresponds more to the rest-frame UV where there are fewer templates available. Thus, we use a simple relation of  $0.004(1+z)$  to estimate the errors (which gives an error of  $0.006$  at our average redshift of  $z \sim 0.5$ ).

## 6. RESULTS

Figures 3–16 show the spectra, all in  $F_2$  units with arbitrary normalization. The top panels show the unsmoothed (or lightly smoothed) spectrum, which typically contains both SN and galaxy light. In the cases in which the SN and galaxy light were

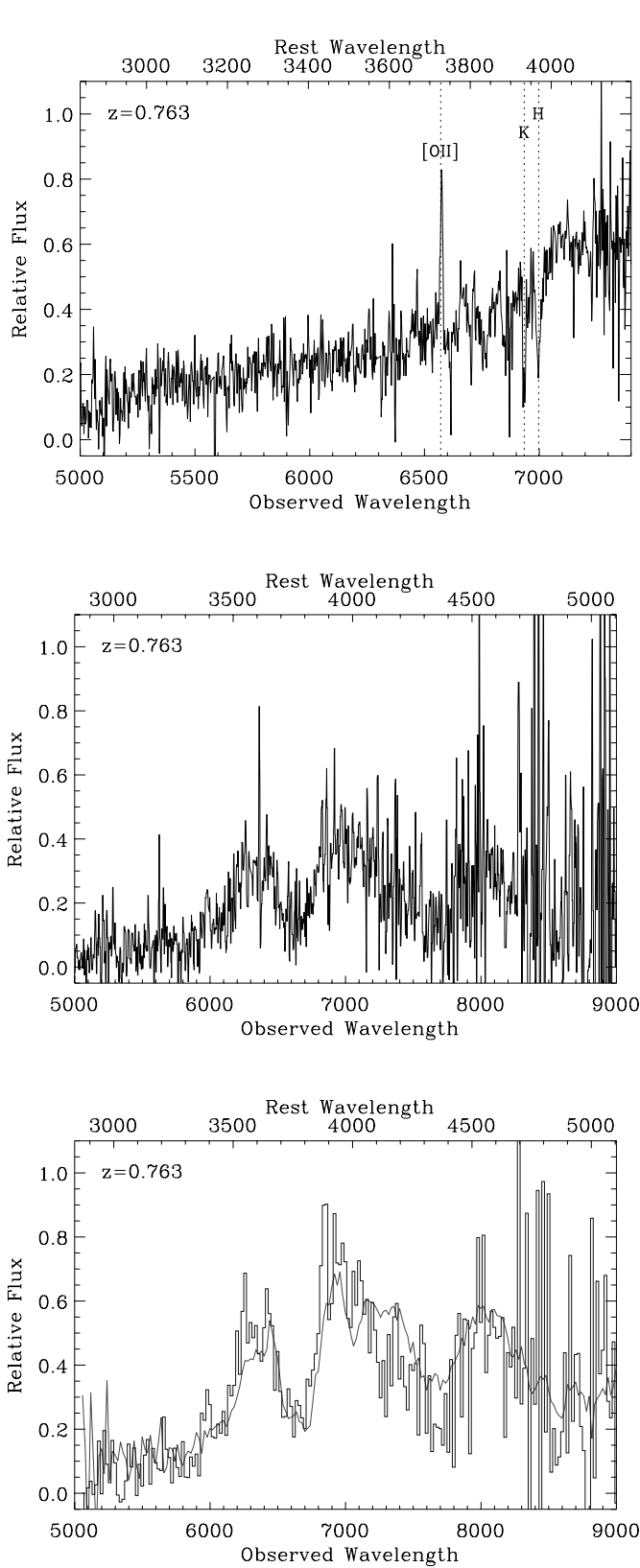


FIG. 4.—*Top*: Lightly smoothed spectrum of neighboring (host) galaxy of SN 1997G (note that atmospheric absorption has not been corrected in this spectrum). *Middle*: Lightly smoothed spectrum of SN 1997G. *Bottom*: Rebinned spectrum of SN 1997G (*histogram*) after interpolating over poorly subtracted sky lines and subtracting an Sa galaxy template, compared with SN 1999bk at +4 days (*solid curve*). [See the electronic edition of the *Journal* for a color version of the bottom panel.]

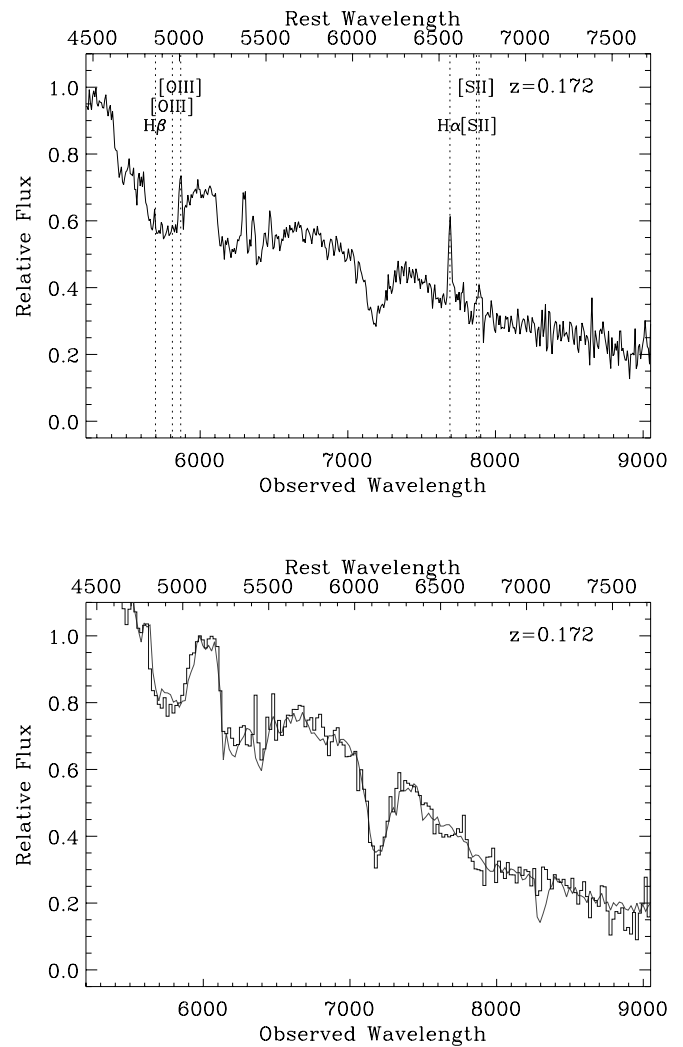


FIG. 5.—*Top*: Unsmoothed spectrum of SN 1997I obtained at the ESO 3.6 m showing galaxy lines used to determine the redshift. *Bottom*: Rebinned spectrum of SN 1997I (*histogram*) after interpolating over narrow galaxy lines and subtraction of an Sb template galaxy spectrum, compared with SN 1999bp at +1 day (*solid curve*). [See the electronic edition of the *Journal* for a color version of the bottom panel.]

resolved and separate extractions were possible, the top panels show the unsmoothed (or lightly smoothed) data for the host galaxy. The bottom panels show the results of the template matching described in the previous section. In almost all cases, clear SN Ia features are visible in the high-redshift SN spectrum.

### 6.1. Notes on Individual Objects

*SN 1997F* (Fig. 3).—This spectrum is a blend of galaxy and SN light (the host galaxy and SN were not separable in the extraction). The host galaxy has  $z = 0.580 \pm 0.001$ , based on narrow lines from [O II], H $\gamma$ , the G band, and [O III]. After subtraction of a galaxy template, broad Ca II is visible. In a SN Ia at this epoch (–7 days), other features are weak, so it is difficult to distinguish them given the S/N of this spectrum. Although the spectrum is dominated by galaxy light, two lines of evidence give us confidence that the residual spectrum is a SN Ia. First, the epoch determined by the fitting program (–6.5 days) agrees well with the epoch determined from the light curve (–7.5 days). Second, a Type Ia is a much better fit to the data than any other SN type.

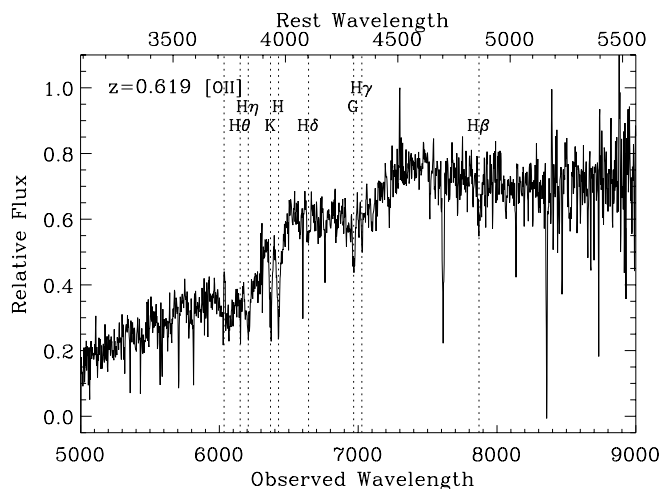


FIG. 6.—*Top*: Unsmoothed spectrum of SN 1997J showing the narrow lines used to determine the redshift. *Bottom*: Rebinning spectrum of SN 1997J (histogram) after subtraction of a template S0 host galaxy, compared with SN 1999bn at day +2 (solid curve). [See the electronic edition of the Journal for a color version of the bottom panel.]

SN 1997G (Fig. 4).—The SN is slightly merged with a brighter galaxy that has  $z = 0.763 \pm 0.001$ . SN Ia features can be seen at the same redshift. The fact that the two objects were merged together made sky subtraction difficult, and residuals remain at observed wavelengths  $\lambda_{\text{obs}} = 5577$  and  $6300 \text{ \AA}$ . These have been interpolated across for the figures. While we consider a Type Ia identification to be the most probable for this SN, a Type Ib/c identification cannot be ruled out due to the lack of definitive Si II and the poor S/N redward of  $\sim 8200 \text{ \AA}$ , corresponding to  $\sim 4650 \text{ \AA}$  in the rest frame. Furthermore, there are few UV spectra of SNe Ib/c, so while the bumps at  $2900$  and  $3150 \text{ \AA}$  (rest frame) observed at  $\sim 5110$  and  $\sim 5550 \text{ \AA}$  match those in a Type Ia, the behavior of SNe Ib/c in this region is not well studied.

SN 1997I (Fig. 5).—The redshift of  $z = 0.172 \pm 0.001$  was derived from galaxy lines (H $\alpha$ , H $\beta$ , S II, and [O III]). The spectrum is an excellent match to SN Ia features, including the  $6150 \text{ \AA}$  Si II feature seen at  $\lambda_{\text{obs}} \sim 7200 \text{ \AA}$  and S II. The identification of this SN as a Type Ia is unambiguous, as the Si II and S II lines can easily be seen.

SN 1997J (Fig. 6).—Narrow absorption lines in the spectrum (Ca II H and K +  $4000 \text{ \AA}$  break from the host galaxy) give

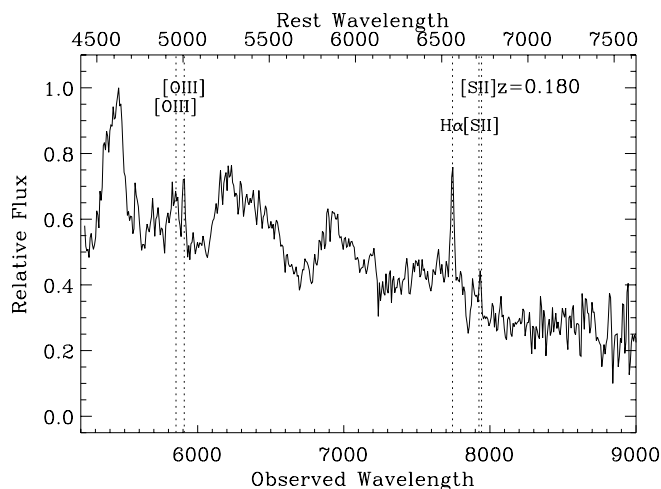


FIG. 7.—*Top*: Unsmoothed spectrum of SN 1997N showing the narrow lines used to determine the redshift. *Bottom*: Rebinning spectrum of SN 1997N (histogram) after interpolating over strong emission lines of [O III] and H $\alpha$  and subtracting template Sb2 host galaxy light, compared with SN 1991T at +15 days (solid curve). [See the electronic edition of the Journal for a color version of the bottom panel.]

$z = 0.619 \pm 0.001$ . SN Ia features at this redshift are clearly visible, despite being affected by the galaxy absorption lines. After subtracting a template S0 galaxy spectrum, the features become much clearer. Here also, the Type Ia identification is most probable but not definitive.

SN 1997N (Fig. 7).—The redshift of  $z = 0.180 \pm 0.001$  was derived from narrow galaxy lines (H $\alpha$ , [O III], and possibly S II). SN Ia features from  $\sim 2$  weeks after maximum are clearly visible in the spectrum, including the Si II  $\lambda 6150$  feature seen at  $\lambda_{\text{obs}} \sim 7250 \text{ \AA}$ . The spectra of the low-redshift SNe SN 1991T and SN 1994D both match this spectrum equally well (see § 7.2).

SN 1997R (Fig. 8).—The host (or a neighboring) galaxy  $2''6$  away has  $z = 0.657 \pm 0.001$  (identified from the Ca H and K lines and the  $4000 \text{ \AA}$  break). The SN shows clear, broad features matching a Type Ia at this redshift, including the  $4000 \text{ \AA}$  Si II feature seen at  $\lambda_{\text{obs}} \sim 6630 \text{ \AA}$ , just redward of the Ca II feature. Narrow lines (H $\eta$ , H $\delta$ , and possibly H $\gamma$ ) are also visible in the spectrum, presumably from the host galaxy.

SN 1997S (Fig. 9).—Narrow lines due to the host galaxy ([O III], [O II], H $\beta$ , and H $\gamma$ ) give  $z = 0.612 \pm 0.001$ . Very clear SN Ia features matching this redshift are visible, including the Ca II, Si II ( $4000 \text{ \AA}$ ), and Fe II features.

*SN 1997ac* (Fig. 10).—The spectrum shows very clear SN Ia features at a redshift of  $z = 0.323 \pm 0.005$  at  $\sim 10$  days after maximum light. Since there are no clear features due to the host galaxy, the redshift is based solely on the SN features. The Si  $\lambda 6150$  feature is clearly visible at an observed wavelength of  $\sim 8100 \text{ \AA}$ , providing an unambiguous identification of the object as a SN Ia.

*SN 1997af* (Fig. 11).—The SN and host galaxy spectra could not be extracted separately. Narrow lines of [O II], Ca H and K,  $H\gamma$ , the G band,  $H\eta$ , and  $H\theta$  due to the host galaxy are clear in the spectrum, giving a redshift of  $z = 0.579 \pm 0.001$ . The spectrum also shows broad features consistent with the spectrum of a SN Ia at the same redshift, including the small Si II feature ( $4000 \text{ \AA}$  rest wavelength) at an observed wavelength of  $\sim 6350 \text{ \AA}$ .

*SN 1997ag* (Fig. 12).—The SN and host galaxy light are blended, and it was not possible to obtain separate extractions. The Ca H and K lines from the host galaxy are visible at  $\lambda_{\text{obs}} = 6266$  and  $6317 \text{ \AA}$ , giving a redshift of  $z = 0.592 \pm 0.001$ . SN Ia features are clearly visible in the spectrum, especially broad Ca II and Fe II.

*SN 1997ai* (Fig. 13).—The spectrum shows very clear SN Ia features at a redshift of  $z = 0.454 \pm 0.006$ . Since there are no clear features due to the host galaxy, the redshift is based solely on the SN features. The lack of host galaxy contamination is confirmed by the fitting program, which used no galaxy light in its fit of the spectrum. The Si II  $\lambda 6150$  feature is clearly visible at an observed wavelength of  $\sim 8900 \text{ \AA}$ , providing an unambiguous identification of the object as a SN Ia.

*SN 1997aj* (Fig. 14).—The SN and host were separated by  $2''.5$  on the slit, and their spectra could be extracted separately. The host galaxy spectrum shows emission lines of [O II], [O III], and  $H\beta$ , as well as absorption lines of  $H\gamma$ ,  $H\delta$ ,  $H\theta$ ,  $H\eta$ , the G band, and Ca H and K, at a redshift of  $z = 0.581 \pm 0.001$ . The SN spectrum is consistent with that of a Type Ia at  $z = 0.581$  showing a strong, broad Fe II  $\lambda 5000$  feature seen at  $\lambda_{\text{obs}} \sim 7900 \text{ \AA}$  but a relatively narrow Ca II  $\lambda 3800$  feature seen at  $\lambda_{\text{obs}} \sim 6000 \text{ \AA}$ .

*SN 1997am* (Fig. 15).—Separate extractions of the host galaxy and SN were possible, since they were separated by  $2''.3$  on the slit. The host galaxy spectrum shows emission lines of [O II],  $H\beta$ , and [O III] at a redshift of  $z = 0.416 \pm 0.001$ . The SN spectrum is a good match to the normal Type Ia SN 1992A spectrum at day +9 and clearly shows the presence of the Si II ( $6150 \text{ \AA}$ ) feature seen at  $\lambda_{\text{obs}} \sim 8710 \text{ \AA}$ . SN 1991T at day +10 is also a good fit to the spectrum (see § 7.2).

*SN 1997ap* (Fig. 16).—The redshift of  $z = 0.831 \pm 0.007$  is based on SN features alone. This spectrum was discussed in detail in Perlmutter et al. (1998). The slightly improved redshift estimate presented here supersedes that of earlier papers (Perlmutter et al. 1998, 1999; Knop et al. 2003). We note here that it was identified as a SN Ia by the presence of both the blue Ca II and Si II features.

## 7. TESTS FOR EVOLUTION

Although these spectra were taken primarily for the purposes of redshift measurement and SN classification, they also allow some basic tests of SN evolution with redshift. We show that SNe Ia do not look dramatically different at high redshift, that they have similar elemental velocities, and that SNe Ia fall into the same subclasses at high redshift.

### 7.1. Spectral Morphology

High-redshift SNe Ia look similar to their low-redshift counterparts, but the implications for constraints on evolution

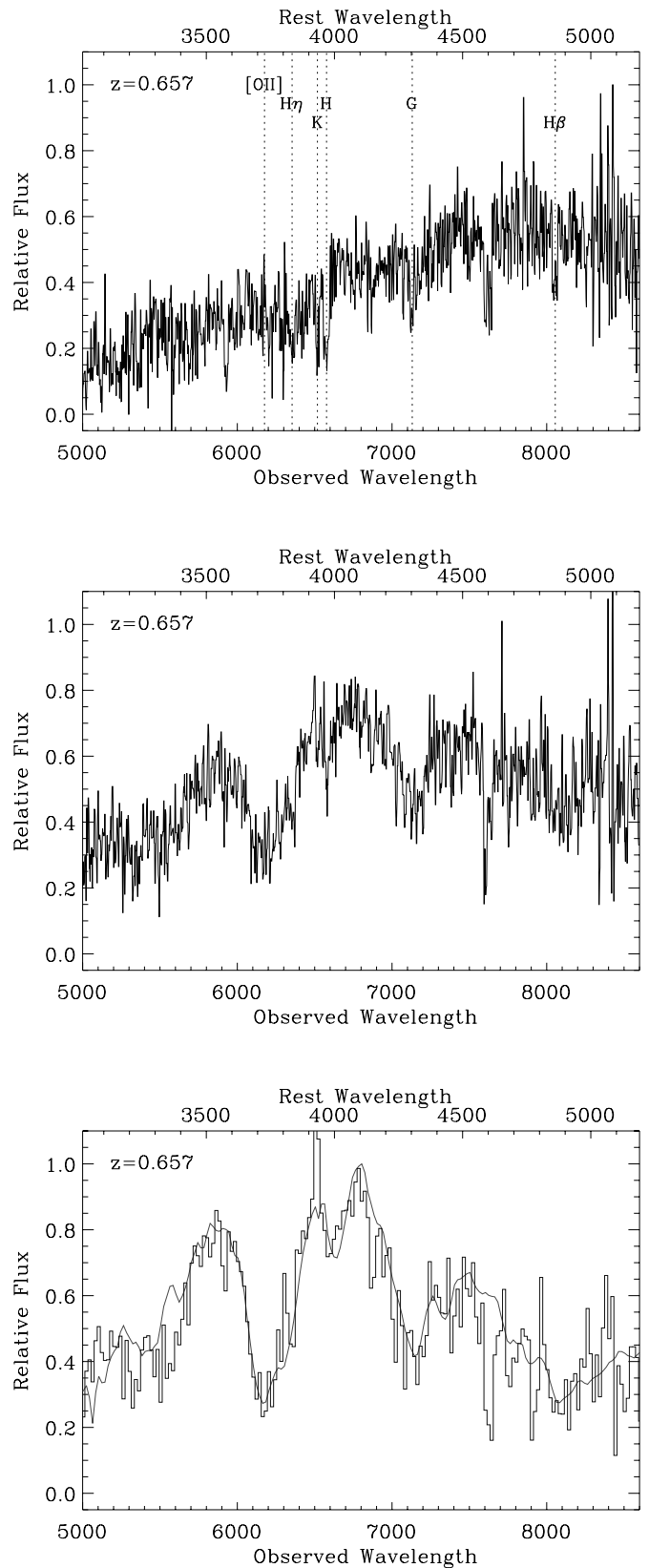


FIG. 8.—*Top*: Lightly smoothed spectrum of the host (or possible neighbor) galaxy of SN 1997R (atmospheric absorption has not been corrected in this spectrum). *Middle*: Lightly smoothed spectrum of SN 1997R. *Bottom*: Re-binned spectrum of SN 1997R (histogram) after interpolating over narrow host galaxy lines, rebinning to  $20 \text{ \AA}$ , and subtracting a template Sa galaxy, compared with SN 1989B at  $-5$  days (solid curve). [See the electronic edition of the Journal for a color version of the bottom panel.]



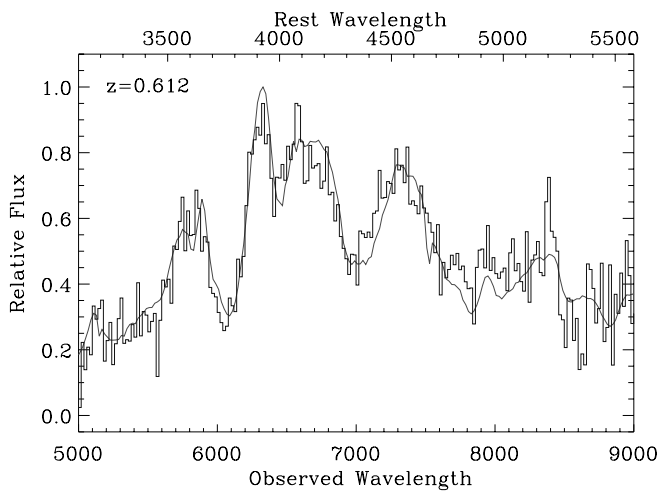
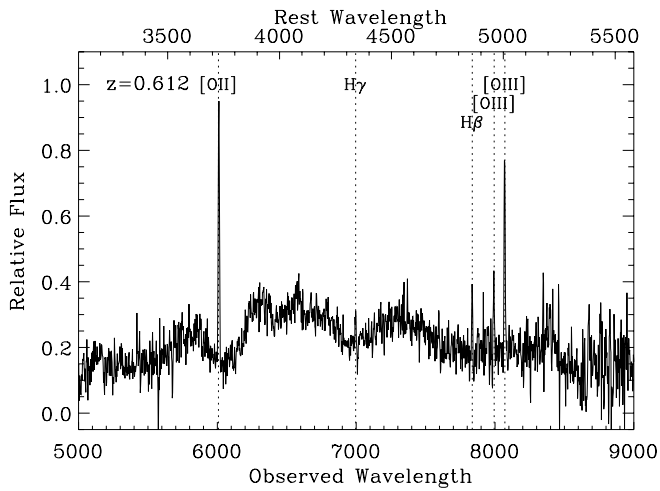


FIG. 9.—*Top*: Unsmoothed spectrum of SN 1997S showing the narrow lines used to determine the redshift. *Bottom*: Rebinned spectrum of SN 1997S (*histogram*) after interpolating over strong emission lines of [O II], [O III], H $\beta$ , and H $\gamma$  and subtraction of an Sb I host galaxy template, compared with SN 1992A at +5 days (*solid curve*). [See the electronic edition of the *Journal* for a color version of the bottom panel.]

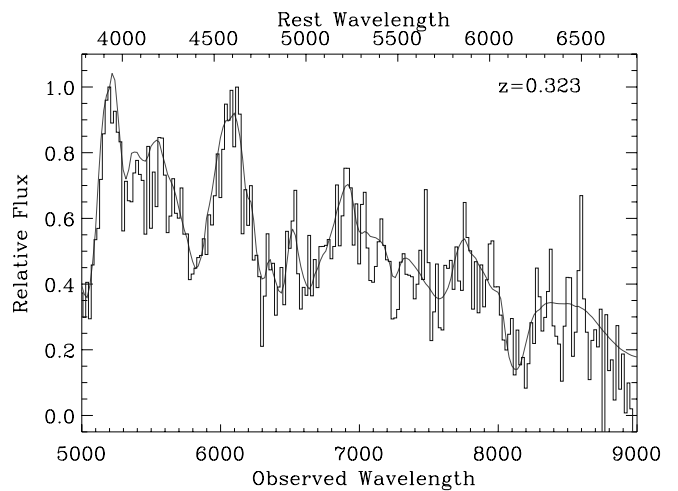
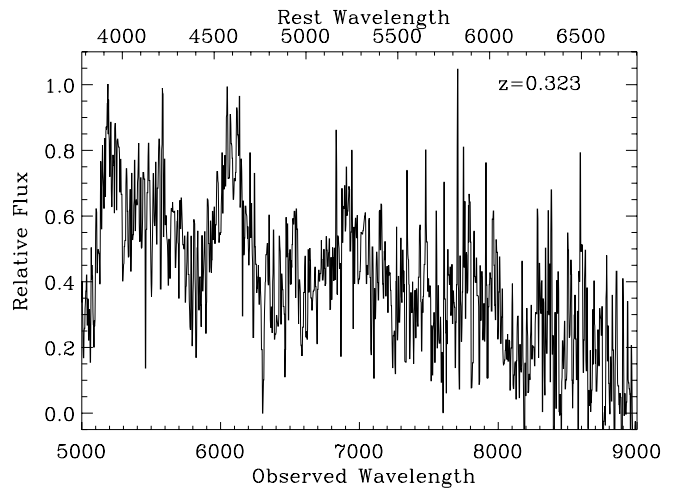


FIG. 10.—*Top*: Lightly smoothed spectrum of SN 1997ac. *Bottom*: Rebinned spectrum of SN 1997ac (*histogram*) compared with SN 1998bu at +11 days (*solid curve*). [See the electronic edition of the *Journal* for a color version of the bottom panel.]

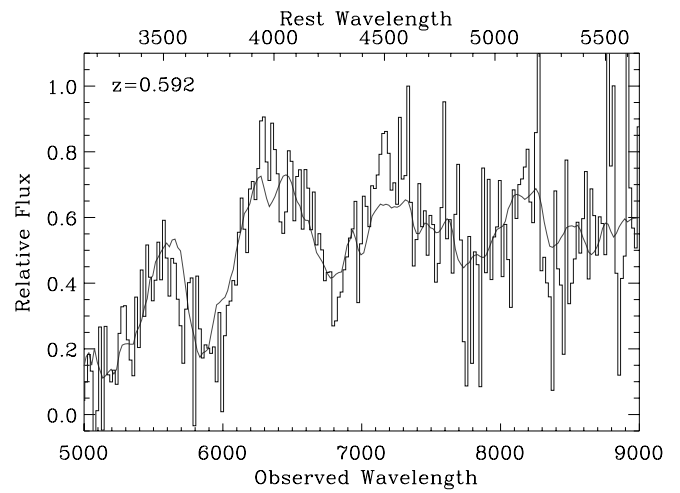
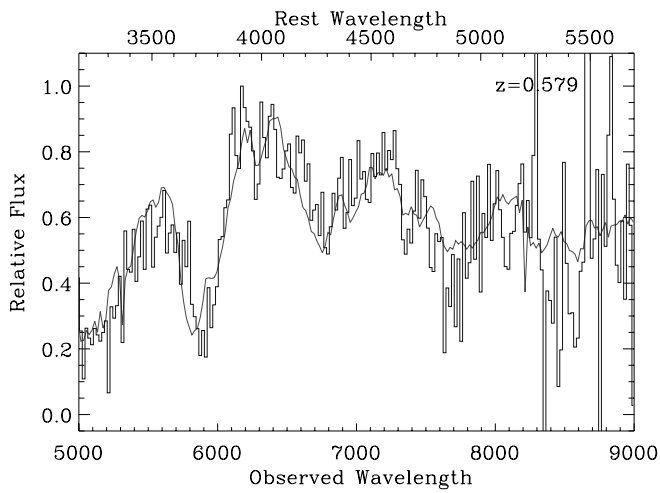
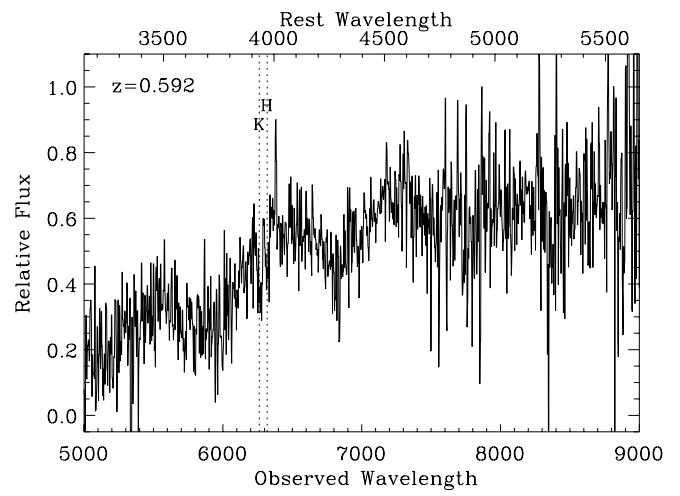
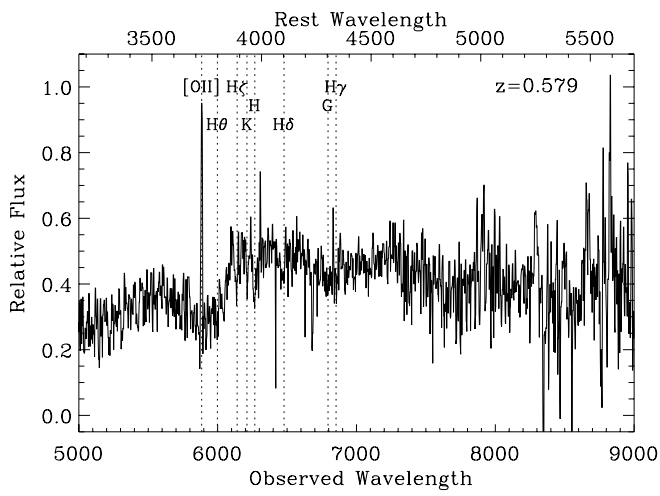


FIG. 11.—*Top*: Unsmoothed spectrum of the host of SN 1997af showing the narrow lines used to determine the redshift. *Bottom*: Rebinned spectrum of SN 1997af (*histogram*) after interpolating across narrow lines from the host galaxy and subtracting an Sb6 galaxy template, compared with the Type Ia SN 1999bp at  $-2$  days (*solid curve*). [See the electronic edition of the *Journal* for a color version of the bottom panel.]

FIG. 12.—*Top*: Lightly smoothed spectrum of SN 1997ag showing narrow features used to determine the redshift. *Bottom*: Rebinned spectrum SN 1997ag (*histogram*) after interpolating over narrow galaxy lines, compared with the Type Ia SN 1990N at  $+7$  days before maximum (*solid curve*). [See the electronic edition of the *Journal* for a color version of the bottom panel.]

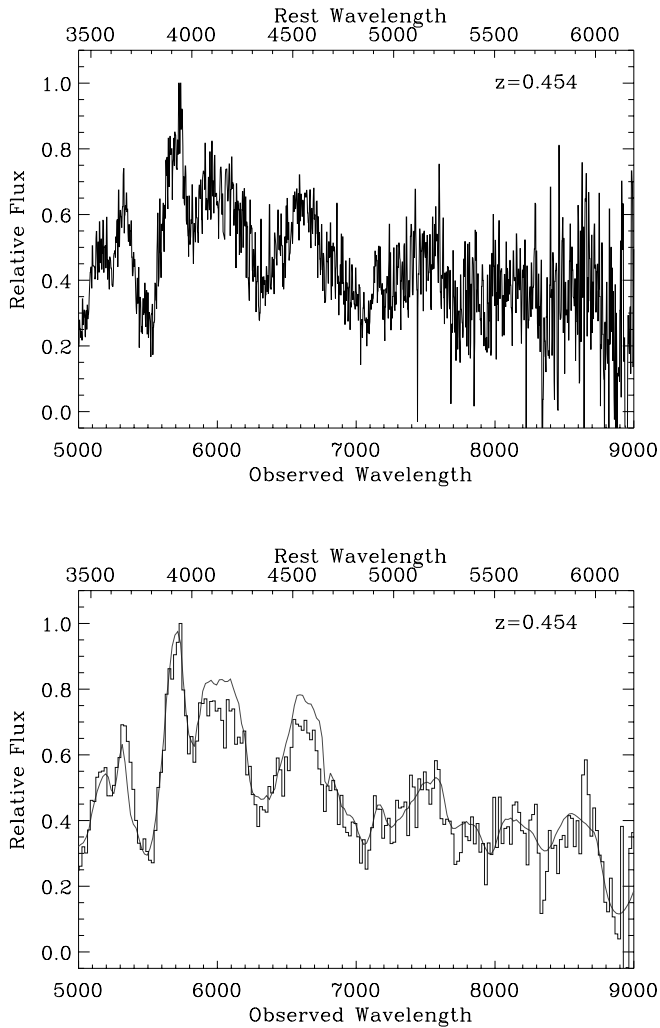


FIG. 13.—*Top*: Lightly smoothed spectrum of SN 1997ai. *Bottom*: Rebinned spectrum of SN 1997ai (*histogram*) compared with the Type Ia SN 1992A at +5 days (*solid curve*). [See the electronic edition of the *Journal* for a color version of the bottom panel.]

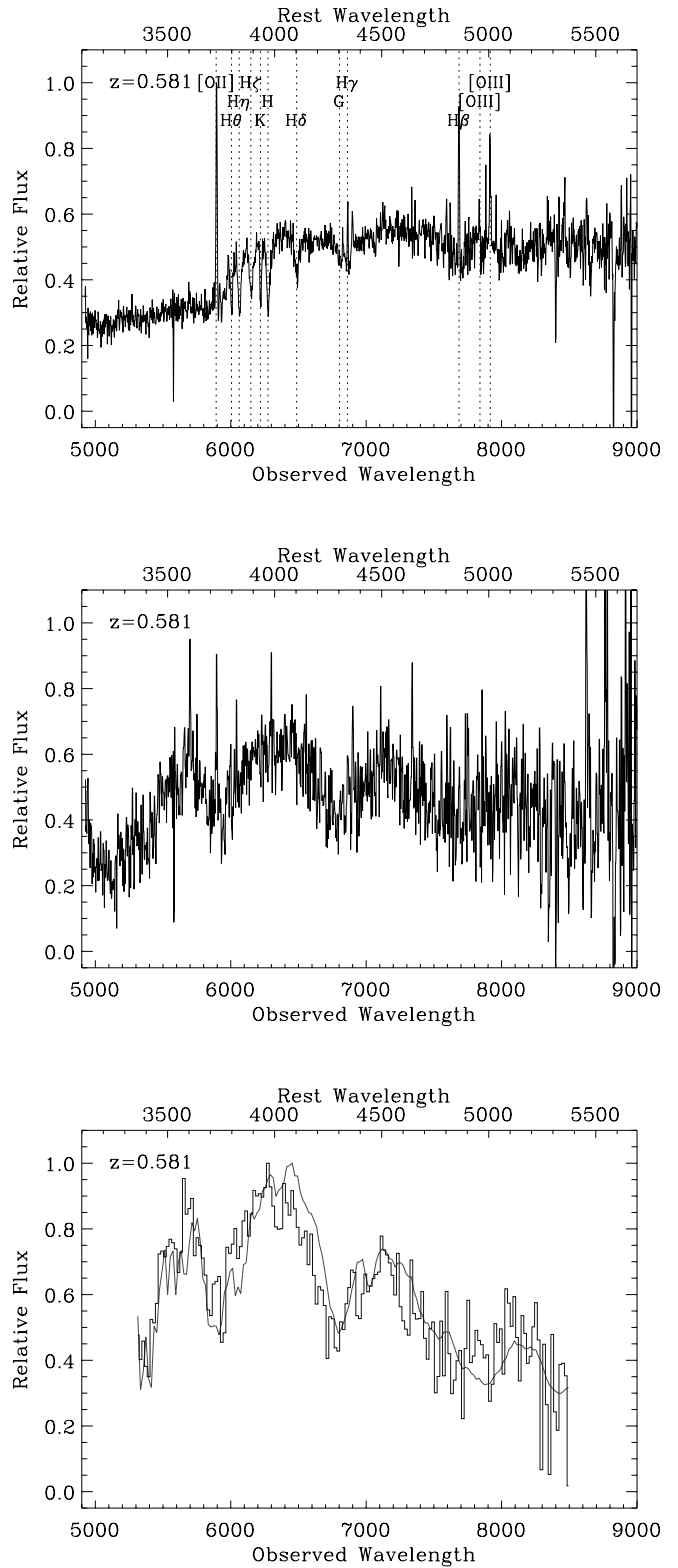


FIG. 14.—*Top*: Unsmoothed spectrum of the host of SN 1997aj (a separate extraction was possible, although there are still narrow galaxy lines in the SN extraction) showing the narrow lines used to determine the redshift. *Middle*: Lightly smoothed spectrum of SN 1997aj. *Bottom*: Rebinned spectrum of SN 1997aj (*histogram*) after interpolating over narrow host galaxy lines of [O II] and Ca H and K and subtracting Sb galaxy light, compared with the Type Ia SN 1999aa at -3 days (*solid curve*). [See the electronic edition of the *Journal* for a color version of the bottom panel.]

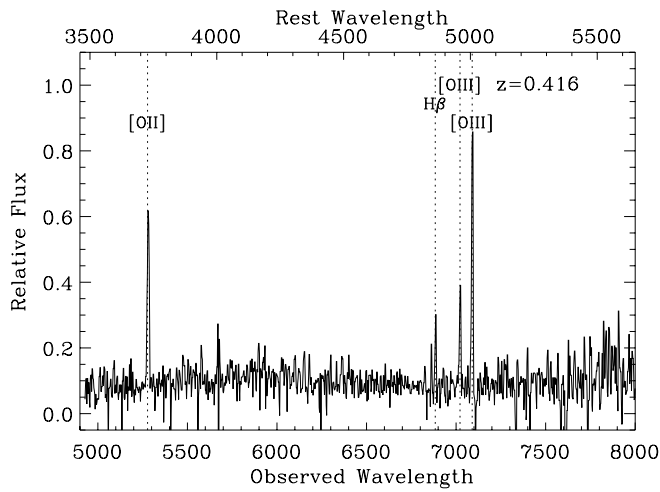


FIG. 15a

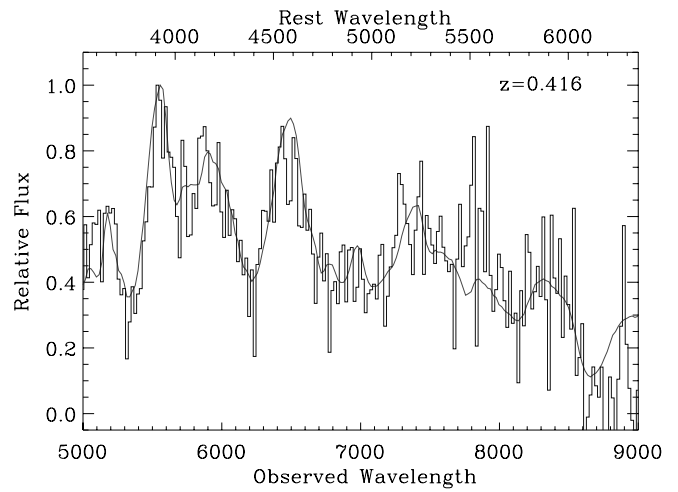


FIG. 15b

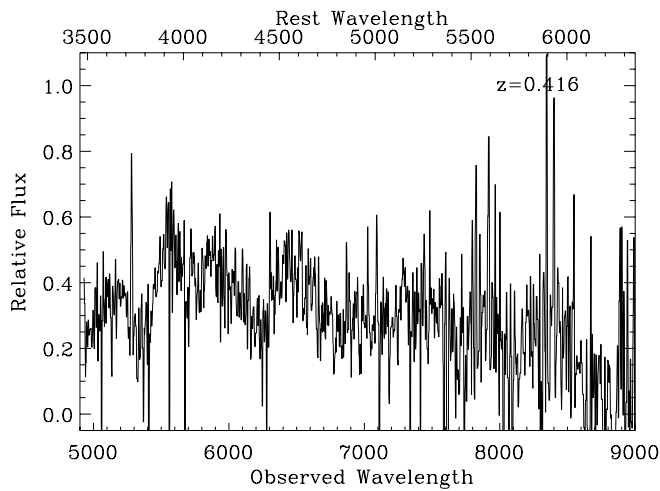


FIG. 15c

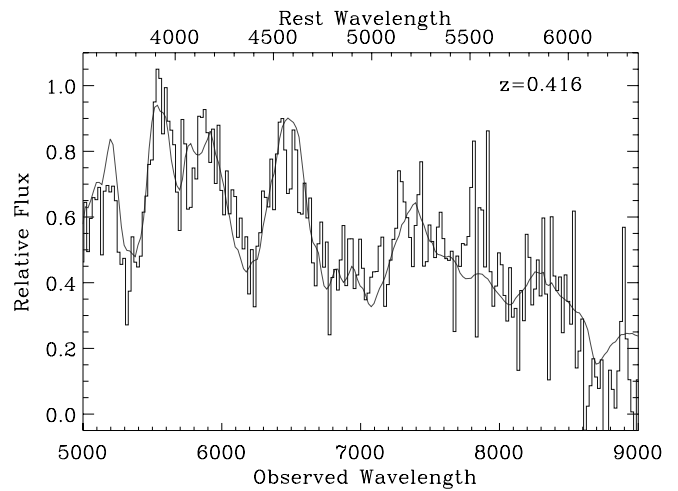


FIG. 15d

FIG. 15.—(a) Unsmoothed spectrum of the host of SN 1997am showing the narrow lines used to determine the redshift. (b) Rebinned spectrum of SN 1997am (histogram) after interpolating across cosmic rays and narrow lines from the host galaxy and subtraction of an Sb1 galaxy template, compared with the Type Ia SN 1992A at +9 days (solid curve). (c) Lightly smoothed spectrum of SN 1997am. (d) Same as (b), but with the Type Ia SN 1991T at +10 days for comparison. [See the electronic edition of the Journal for a color version of panels b and d.]

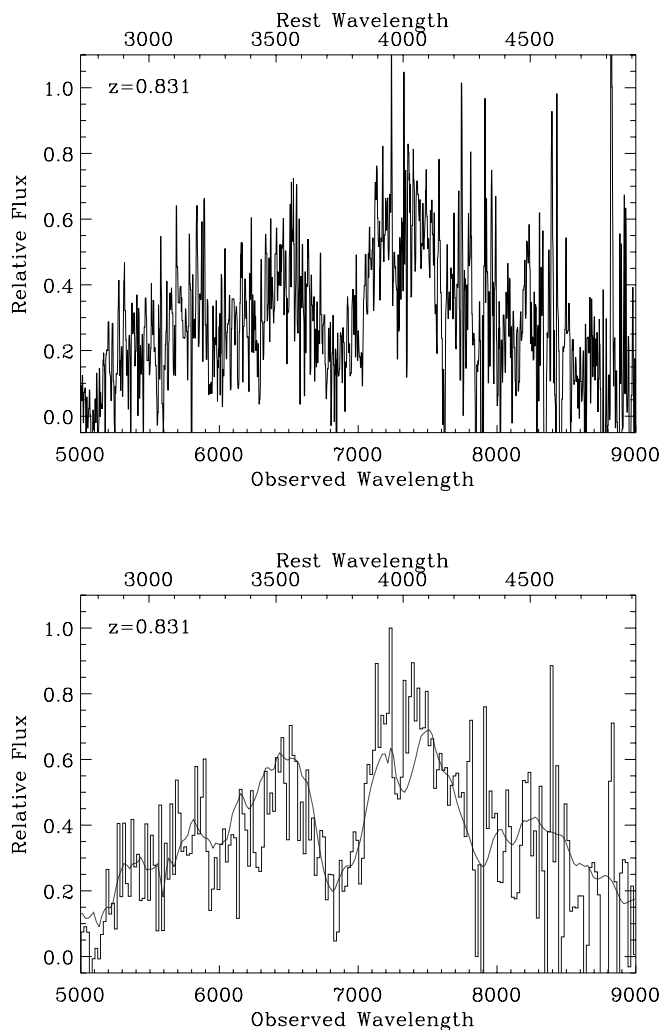


FIG. 16.—*Top*: Lightly smoothed spectrum of SN 1997ap. *Bottom*: Re-binned spectrum of SN 1997ap (histogram) after interpolating across the sky absorption region at 7600 Å compared with the Type Ia SN 1989B at  $-5$  days (solid curve). [See the electronic edition of the *Journal* for a color version of the bottom panel.]

are complicated. Figure 17 shows a selection of the high-redshift spectra (those not significantly contaminated by host galaxy light) plotted in order of rest-frame days past maximum. These are interspersed with the time sequence for the nearby Branch-normal SN Ia SN 1992A. Note that because the high-redshift spectra are not spectrophotometric measurements (see §§ 3 and 5.2), differences in the overall slope of the spectra should not be considered significant. Despite the lower S/N of the high-redshift spectra and the nonuniform wavelength coverage (since the spectra have been deredshifted by different amounts), it is clear that the overall trends in the spectral evolution with light-curve phase are the same at low and high redshift. Furthermore, Figures 3–16 show that high-redshift SNe resemble well-observed local SNe on an object-by-object basis.

### 7.2. The Incidence of Spectroscopically Peculiar SNe

Li et al. (2001a, 2001b) make the case that, while slowly declining, spectroscopically peculiar SNe like SN 1991T and SN 1999aa represent 20% of SNe discovered in volume-limited local surveys, they are strangely absent from high-redshift SN samples. This is paradoxical, since these SNe are overluminous

and so should be seen in *greater* numbers in flux-limited surveys. The authors present one possible solution: that these SNe become spectroscopically normal with time and appear normal by the time spectra are taken.

Perhaps supporting this idea, for two of our cases, both taken at relatively late times after maximum light, the spectrum of SN 1991T fits as well as the spectrum of a more normal SN. SN 1997am has a light-curve stretch (a measure of the rise and decline time of the SN light curve, defined in Perlmutter et al. 1999) of  $s = 1.03 \pm 0.06$  (Knop et al. 2003), which is consistent with the stretch of SN 1991T ( $s = 1.08$ ). Since the spectrum was taken approximately 10 rest-frame days after maximum light, by which time SN 1991T itself appears to be fairly spectroscopically normal, there is no definitive spectroscopic evidence that SN 1997am is a peculiar Type Ia, but it cannot be ruled out. In the other case, SN 1997N, the spectrum was taken approximately 16 rest-frame days after maximum. It is possible that this SN looked spectroscopically similar to SN 1991T at early times, although again there is no definitive spectroscopic evidence for this. The stretch of SN 1997N is  $s = 1.03 \pm 0.02$ , somewhat lower than that of SN 1991T. However, we note that the nearby SN 1997br also resembled SN 1991T spectroscopically yet had a fairly normal light curve, with  $\Delta m_{15}(B) = 1.00 \pm 0.15$ ,  $s = 1.04$  (Li et al. 1999). Garavini et al. (2005) have found definitive evidence for a SN 1991T-like SN at high redshift. In that case the spectrum was taken 7 days before maximum, when the spectral peculiarities are more evident.

The explanation for the supposed dearth of SN 1991T-like SNe at high redshift proposed by Li et al. (that they are in the data set but appear spectroscopically normal when spectra are taken) appears to be part of the answer to the paradox, although the situation may be more complicated. These SNe may not be as consistently overluminous as first thought (Li et al. 1999; Saha et al. 2001; Gibson & Stetson 2001); thus, Li et al. (2001a) may have overpredicted the expected numbers in a flux-limited survey.

At the other extreme, spectroscopically peculiar, underluminous SNe like SN 1991bg (Filippenko et al. 1992; Leibundgut et al. 1993; Turatto et al. 1996) and SN 1999by (Toth & Szabó 2000; Howell et al. 2001; Vinkó et al. 2001; Höflich et al. 2002) have not been seen at high redshift. While it is unlikely that these SNe will be found in flux-limited searches, it is also possible that these SNe are from such an old stellar population that they do not exist at  $z > 0.5$  (Howell 2001).

### 7.3. Calcium Velocities

While the depth of absorption lines gives some information about the quantity of an ion in a SN, the velocity of the line gives information about the ion's distribution within the photosphere. Furthermore, the velocity of the SN ejecta is related to the overall kinetic energy of the event. The kinetic energy has a direct influence on the opacities and hence on the total brightness of the SN and its light-curve shape.

In Figure 18 we present a plot of the velocities of the Ca II minima for the SCP high-redshift SNe compared with two well-observed nearby SNe. We note that while the absorption feature at 3700 Å is dominated by Ca II, Si II and various ionization states of the iron peak elements (see Hatano et al. 1999) also contribute. For the three lowest redshift SNe in the SCP set, the Ca II feature is outside the observed wavelength range. Therefore, this analysis is restricted to the SCP SNe with  $z > 0.38$ .

The analysis was performed on the spectra after galaxy subtraction had been done, if this was necessary (as described in § 6). The Ca II velocities were estimated by fitting a Gaussian

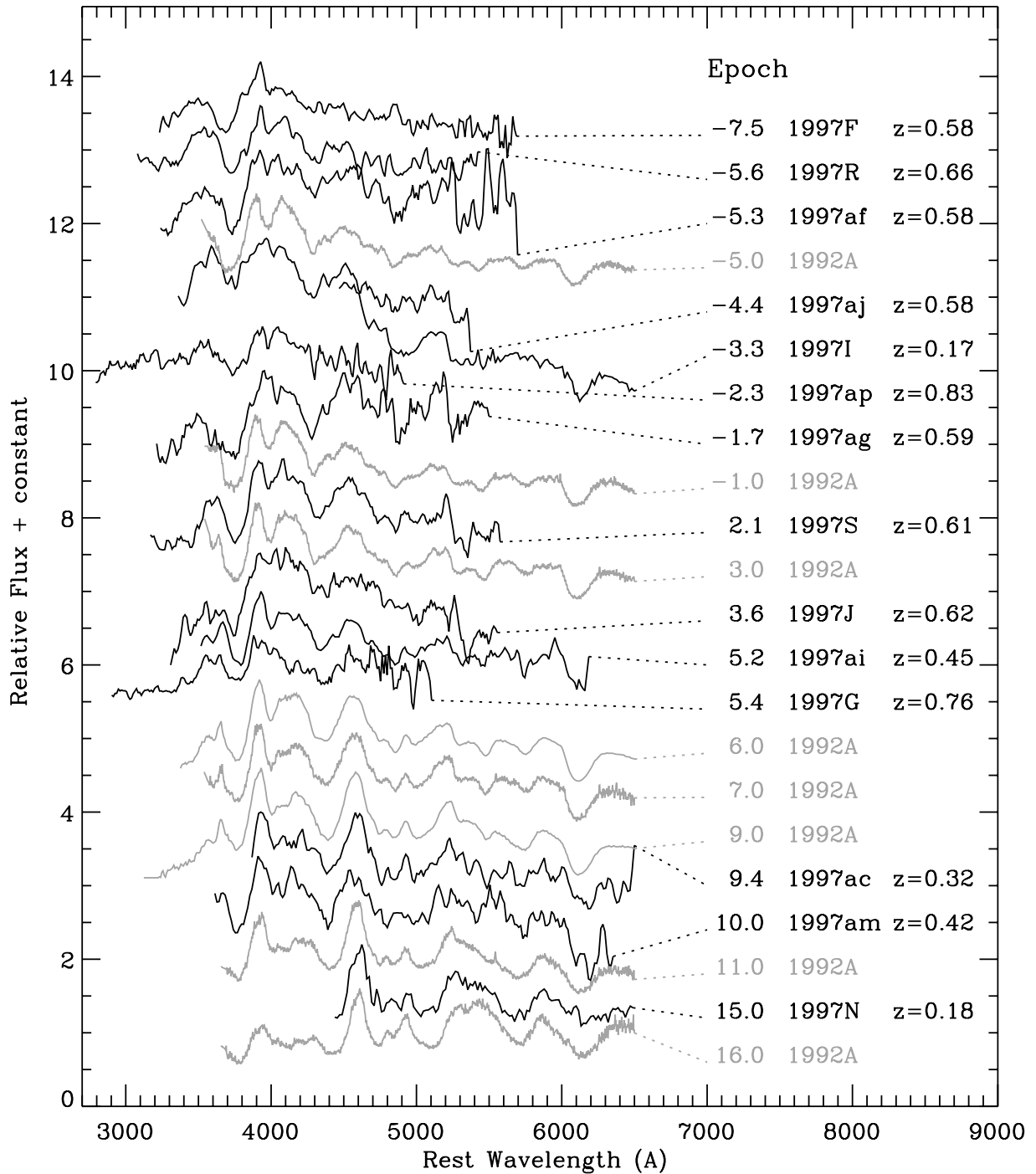


FIG. 17.—Time sequence of high-redshift SN spectra in order of rest-frame date relative to maximum light, as determined from the light curve ( $\tau_{lc}$ ). Spectra of the nearby Type Ia SN 1992A are interspersed for comparison. [See the electronic edition of the *Journal* for a color version of this figure.]

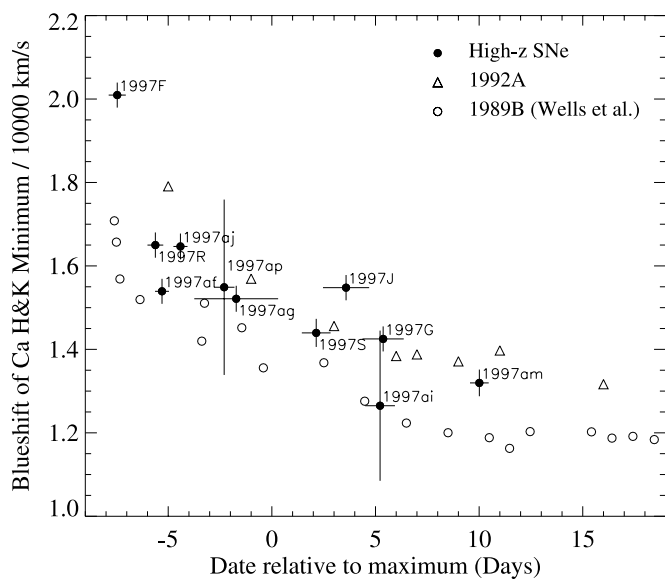


FIG. 18.—Comparison of the velocities determined for the minima of the Ca II feature for two well-observed nearby SNe Ia (1992A and 1989B) and the high-redshift SNe presented in this paper.

function to the region 3610–3870 Å in the rest frame, followed by a second iteration using the region from  $-65$  to  $+100$  Å either side of the previous estimate of the minimum. The velocity shift was calculated from the wavelength of the minimum by assuming a rest-frame wavelength for this feature of 3945.28 Å. The same analysis was done on a spectral series for the normal Type Ia SN 1992A (Kirshner et al. 1993). Finally, the published Ca II velocities for the normal Type Ia SN 1989B (Wells et al. 1994) are also shown.

The general trend of decreasing Ca II velocities as a function of time and the range in velocities at a given epoch seen in the data is completely consistent with the range seen in nearby observations. This result is confirmed by Garavini et al. (2005) in a more recent independent set of high-redshift SN spectra.

Our high-redshift data are also broadly consistent with the recent study of nearby SNe by Benetti et al. (2005), although the comparison is complicated by the fact that Benetti et al. measure Si II velocities, whereas we consider Ca II velocities. Taking into account the apparent offset between the two (as can be seen from SN 1992A and SN 1989B, for example), the velocities seen in our high-redshift sample (including the large value for SN 1997F) are broadly consistent with the range of velocities seen in nearby SNe. Because of the larger error bars at high redshift and only having a single velocity measurement per SN, it is not possible to determine into which of the Benetti et al. (2005) classes each of our objects would fall.

## 8. CONCLUSIONS

At the present time, the statistical and systematic errors in the measurement of the cosmological parameters from Type Ia supernovae (SNe Ia) are of similar size. As the quality and quantity of high-redshift SN observations grows, it will become even more important to constrain the systematic uncertainties. Non-Ia contamination and evolution are two of the larger potential systematics we currently face. Here we have presented some of the methods we employ to reduce/study these uncertainties.

In this paper we have presented spectra for 14 high-redshift SNe and demonstrated that the spectra are consistent with Type Ia. In three cases at intermediate redshift (SN 1997ac, SN 1997ai,

and SN 1997am at  $z \sim 0.3$ – $0.5$ ), in addition to two at lower redshift (SN 1997I and SN 1997N), we have observed the Si II  $\lambda 6150$  feature and hence have unambiguously identified the SN as Type Ia. For higher redshifts, this Si II feature becomes increasingly difficult to observe, as fringing and poor CCD response in the red and bright OH lines in the sky background make the spectra very noisy redward of  $\sim 9500$  Å. Here we have used spectral matching combined with the identification of specific spectral features to identify the objects as SNe Ia, the most important being the identification of Si II features near 4000 Å.

We have carried out first-order quantitative tests to compare the high-redshift spectra with their low-redshift counterparts. We show that the spectral phase determined from spectral matching to low-redshift Type Ia spectra is in very good agreement with the phase determined from the high-redshift light curve. Similarly, the spectral time series shows the same overall trends at low and high redshift. Finally, quantitative measurements of the calcium ejection velocity in the high-redshift spectra are also consistent with those measured from the spectra of low-redshift Branch-normal SNe Ia. Therefore, we have found no evidence for evolution in the population of SNe Ia up to redshifts of  $z \sim 0.8$ . While we cannot prove that all SNe Ia at high redshift are identical to their low-redshift counterparts, we can say that it is possible to choose a set of high-redshift SNe Ia that are equivalent to their low-redshift counterparts to within the accuracy of these quantitative tests.

With larger samples, such as those now being collected by the Supernova Legacy Survey (Pritchett 2005) and the ESSENCE project (Matheson et al. 2005 and references therein), it will be possible to make more detailed comparisons in smaller redshift bins in the range  $0.2 < z < 1$  and in subsets based on light-curve stretch, galaxy host type, and other factors. Such studies will provide further confidence in the use of SNe Ia as distance indicators, and, in cases in which quantitative measurements of spectral features are found to correlate with luminosity or light-curve stretch (e.g., Nugent et al. 1995; Folatelli 2004), these can be used to reduce scatter in the Hubble diagram and thus improve the precision to which cosmological parameters may be measured.

The authors acknowledge the help of the night assistants and support staff at the telescopes from which data for this paper were obtained. We thank the anonymous referee for a very thorough reading of the paper and helpful suggestions.

This paper makes use of light-curve photometry collected at the Cerro Tololo Inter-American Observatory, which is operated by the Association of Universities for Research in Astronomy (AURA), Inc., under a cooperative agreement with the National Science Foundation. This paper is based in part on observations obtained at the WIYN Observatory, which is a joint facility of the University of Wisconsin—Madison, Indiana University, Yale University, and the National Optical Astronomy Observatory. We also make use of observations made with the NASA/ESA *Hubble Space Telescope*, obtained at the Space Telescope Science Institute, which is operated by AURA, Inc., under NASA contract NAS 5-26555. These observations are associated with programs DD-7590 and GO-7336.

This work was supported in part by the Royal Swedish Academy of Sciences and by the Director, Office of Science, Office of High Energy and Nuclear Physics, of the US Department of Energy under contract DE-AC03-76SF00098. Support for this work was provided by NASA through grant HST-GO-7336 from the Space Telescope Science Institute.

## REFERENCES

- Baldwin, J. A., & Stone, R. P. S. 1984, *MNRAS*, 206, 241  
Barris, B. J., et al. 2004, *ApJ*, 602, 571  
Benetti, S., et al. 2005, *ApJ*, 623, 1011  
Buzzoni, B., et al. 1984, *Messenger*, 38, 9  
Cappellaro, E., Turatto, M., & Fernley, J. 1995, IUE-ULDA Access Guide No. 6: Supernovae (ESA-SP 1189; Noordwijk: ESA)  
Cardelli, J. A., Clayton, G. C., & Mathis, J. S. 1989, *ApJ*, 345, 245  
Clocchiatti, A., Wheeler, J. C., Brotherton, M. S., Cochran, A. L., Wills, D., Barker, E. S., & Turatto, M. 1996, *ApJ*, 462, 462  
Coil, A. L., et al. 2000, *ApJ*, 544, L111  
Filippenko, A. V. 1997, *ARA&A*, 35, 309  
Filippenko, A. V., et al. 1992, *AJ*, 104, 1543  
Folatelli, G. 2004, Ph.D. thesis, Stockholm Univ.  
Garavini, G., et al. 2005, *A&A*, submitted  
Garnavich, P., et al. 1998, *ApJ*, 509, 74  
Gibson, B. K., & Stetson, P. B. 2001, *ApJ*, 547, L103  
Hamuy, M. 1994, *PASP*, 106, 566  
Hatano, K., Branch, D., Fisher, A., Millard, J., & Baron, E. 1999, *ApJS*, 121, 233  
Höflich, P., Gerardy, C. L., Fesen, R. A., & Sakai, S. 2002, *ApJ*, 568, 791  
Howell, D. A. 2001, *ApJ*, 554, L193  
Howell, D. A., Höflich, P., Wang, L., & Wheeler, J. C. 2001, *ApJ*, 556, 302  
Howell, D. A., & Wang, L. 2002, *BAAS*, 34, 1256  
Kinney, A. L., Bohlin, R. C., Calzetti, D., Panagia, N., & Wyse, R. F. G. 1993, *ApJS*, 86, 5  
Kirshner, R., et al. 1993, *ApJ*, 415, 589  
Knop, R., et al. 2003, *ApJ*, 598, 102  
Leibundgut, B., et al. 1993, *AJ*, 105, 301  
Li, W., Filippenko, A. V., & Riess, A. G. 2001a, *ApJ*, 546, 719  
Li, W., Filippenko, A. V., Treffers, R. R., Riess, A. G., Hu, J., & Qiu, Y. 2001b, *ApJ*, 546, 734  
Li, W. D., et al. 1999, *AJ*, 117, 2709  
Lidman, C., et al. 2005, *A&A*, 430, 843  
Matheson, T., et al. 2005, *AJ*, 129, 2352  
Meikle, W. P. S., et al. 1996, *MNRAS*, 281, 263  
Nugent, P., Phillips, M., Baron, E., Branch, D., & Hauschildt, P. 1995, *ApJ*, 455, L147  
O'Donnell, J. E. 1994, *ApJ*, 422, 158  
Oke, J. B., & Gunn, J. E. 1983, *ApJ*, 266, 713  
Oke, J. B., et al. 1995, *PASP*, 107, 375  
Perlmutter, S., et al. 1995, *ApJ*, 440, L41  
———. 1997, in *Thermonuclear Supernovae*, ed. P. Ruiz-Lapuente, R. Canal, & J. Isern (Dordrecht: Kluwer), 749  
———. 1998, *Nature*, 391, 51  
———. 1999, *ApJ*, 517, 565  
Pritchett, C. J. 2005, in *ASP Conf. Ser. 339, Observing Dark Energy*, ed. S. C. Wolff & T. R. Lauer (San Francisco: ASP), 60  
Richardson, D., Thomas, R., Casebeer, D., Branch, D., & Baron, E. 2002, *BAAS*, 34, 1205  
Riess, A. G., et al. 1998, *AJ*, 116, 1009  
———. 2004, *ApJ*, 607, 665  
Saha, A., Sandage, A., Thim, F., Labhardt, L., Tammann, G. A., Christensen, J., Panagia, N., & Macchetto, F. D. 2001, *ApJ*, 551, 973  
Schmidt, B. P., et al. 1998, *ApJ*, 507, 46  
Stone, R. P. S., & Baldwin, J. A. 1983, *MNRAS*, 204, 347  
Sullivan, M., et al. 2003, *MNRAS*, 340, 1057  
Tonry, J. L., et al. 2003, *ApJ*, 594, 1  
Toth, I., & Szabó, R. 2000, *A&A*, 361, 63  
Turatto, M., Benetti, S., Cappellaro, E., Danziger, I. J., della Valle, M., Gouiffes, C., Mazzali, P. A., & Patat, F. 1996, *MNRAS*, 283, 1  
Vinkó, J., Kiss, L. L., Csák, B., Fűrész, G., Szabó, R., Thomson, J. R., & Mochnacki, S. W. 2001, *AJ*, 121, 3127  
Wells, L. A., et al. 1994, *AJ*, 108, 2233